

Qualifying Fingerprint Samples Captured by Smartphone Cameras in Real-Life Scenarios

Guoqiang Li, Bian Yang and Christoph Busch

Norwegian Information Security Laboratory, Norwegian University of Science and Technology, Norway

Email: {guoqiang.li, bian.yang, christoph.busch}@ntnu.no

Abstract — While biometrics has been extensively adopted by industry and governments for identification and forensics purposes relying on dedicated biometric sensors and systems, the consumer market driven by innovations in consumer electronics (smartphones, tablets, etc.) is believed to be the next sector that biometric technologies can find wider applications. Compared to dedicated biometric sensors, the sensors embedded in such general-purposed devices may suffer from sample quality instability, which has significant impact on biometric performance. The concern on sample quality may jeopardize the market confidence in consumer devices for biometric applications. In this paper, we propose an approach to assessing the quality of fingerprint samples captured by smartphone cameras under real-life uncontrolled environments. Our approach consists of a sample processing pipeline during which a sample is divided into blocks and a set of local quality features are extracted from each block, including 3 pixel-based features, 4 autocorrelation based features, and 5 frequency features from the autocorrelation result. Afterwards, a global sample quality score is calculated by fusing all image blocks' qualification status. Thanks to the extracted features' capability in discriminating high-quality foreground (fingerprint area) blocks from low-quality foreground ones and background ones, the proposed approach does not require foreground segmentation in advance and thus we call it a one-stop-shop approach. Experiments compare the proposed approach with NFIQ and the proposed pipeline using standardized quality features, and demonstrate our approach's better performance in qualifying smartphone-camera fingerprint samples¹.

Index Terms — fingerprint recognition, sample quality assessment, smartphone camera, autocorrelation.

I. INTRODUCTION

Biometrics [1] has widely adopted for identification purpose (to verify or to search for the identity of an individual) and forensics purpose (to collect and compare biometric traits as legal evidence). As the most widely-adopted (e.g., by ICAO [2] for ePassport) biometric modality for governmental and industrial applications, fingerprint recognition has been standardized by ISO [3; 4] and nowadays deployed in many identity management solutions. While fingerprint has been extensively used and enabled by dedicated biometric sensors and systems, the consumer market driven by innovations in consumer-oriented mobile devices (smartphone, tablet, smart-watch, Google Glass, etc.) in recent years is opening an even

wider market for fingerprint technologies enabled by such general-purposed mobile devices. These general-purposed mobile devices, when adopted for different biometric applications, e.g., device access control [5; 6], remote identity authentication [7; 8], or simply a biometric reader, may have advantages in portability, costs, state-of-the-art sensor integration, multi-functional integration, interface compatibility, convenience to use, and even privacy for personal use both technically and psychologically, since the device as a biometric reader is always under the owner's control. These integrated general purposed sensors (camera, microphone, accelerometer, etc.) show potential to be exploited as biometric sensors. However, the sample quality, which has significant impact on biometric performance [9], rendered by such embedded or plug-in sensors (e.g., the fingerprint samples captured by a smartphone built-in camera in an uncontrolled environment) is usually less stable compared to the case using dedicated biometric sensors. This concern on sample quality may jeopardize the market confidence in such general-purposed mobile devices, especially those popular consumer electronics, for biometric use.

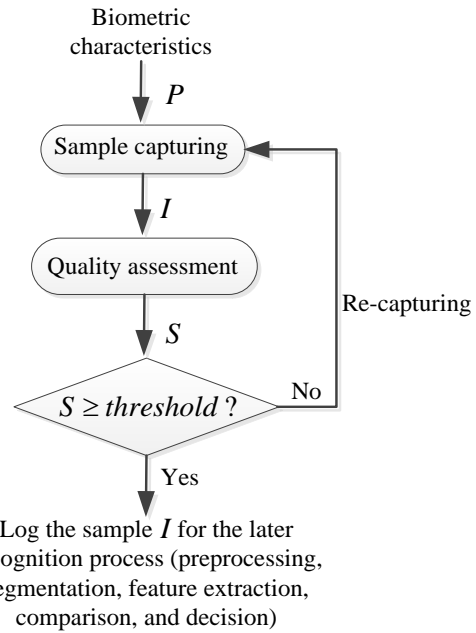


Fig. 1. A general process of biometric sample quality control (P: probe; I: captured sample; S: quality score)

To ensure that a biometric system is operated with high accuracy performance (i.e., low error rates), sample must be

¹ This work is funded under grant agreement 284862 for the EU-FP7 large-scale integrated project FIDELITY (www.fidelity-project.eu/).

carefully controlled in quality during the capturing phase. Fig. 1 gives a generic workflow for sample quality control in a biometric system, where the quality assessment function is the key part to the whole process. Sample quality control ensures that a captured sample has enough quality for the following recognition process in the sense that both the FTA (fail-to-acquire) rate [10] for features generation and the FTE (fail-to-enroll) rate [10] for reference generation can be minimized as well as biometric recognition accuracy being maximized. Since the quality control process takes iterations before logging a qualified sample, a computationally-efficient quality assessment approach is always desired, especially for mobile devices.

For fingerprint samples, various quality assessment approaches have been studied [9; 11; 12; 13; 14; 15] and standardized [16] but all these approaches are limited in scope to samples generated from dedicated fingerprint sensors, i.e., touch-based sensors or environment-controlled touchless sensors, which generates a fairly clean background and a high-contrast foreground (i.e., ridge patterns) such as the example in Fig. 2 (a). However, samples captured by a general-purposed smartphone camera look so different, such as the example in Fig. 2 (b), that existing sample quality assessment approaches may not work in this case. This drove us to investigate the feasibility of the existing approaches on smartphone-camera samples and, if they being proved infeasible or less performed, to propose new approaches to address the new challenge brought by such smartphone cameras.

To test the quality of smartphone-camera fingerprint samples, we created a database with samples collected from 3 widely-used smartphones under various real-life scenarios. Both biometric performance testing and sample quality assessment were done on this database. A new one-stop-shop approach is proposed and compared to some traditional approaches in sample quality assessment. As a pilot study on this topic, our work described in this paper has the following merits:

- (1) A real-life scenario smartphone-camera fingerprint database was established containing samples in large quality variance, which could be, as far as we know, the first database of this type in the biometric research society;
- (2) A one-stop-shop pipeline was proposed for sample quality assessment without needing computationally-intensive foreground (fingerprint area) segmentation for quality-challenged (complicate background or ill-illuminated) samples;
- (3) Differential-autocorrelative-integration (DAI), an efficient block ridge pattern descriptor, was proposed to extract quality features with high discriminability;
- (4) Metrics were suggested for evaluating the performance of sample quality assessment methods suitable for smartphone-camera fingerprint samples.

The remaining part of this paper is arranged as follows. Section 2 gives background on the fingerprint sample quality assessment, unique characteristics of smartphone-camera samples, and the challenges to existing fingerprint quality

assessment approaches. Section 3 proposes our one-stop-shop pipeline, which is designed to cope with the said challenges, tailors some quality metrics used for samples generated from dedicated sensors, and proposes new quality metrics to better suit the smartphone-camera fingerprint samples. Section 4 introduces the real-life smartphone camera fingerprint database this paper established and the experimental settings for performance testing of the proposed quality assessment approach. Section 5 presents testing results with comparison to some typical quality features designed for traditional fingerprint samples. Section 6 concludes this paper.

II. BACKGROUND INFORMATION

A. Fingerprint sample quality: concept and methodology

Biometric sample quality has significant impact on a biometric system's recognition performance [9]. This is because the performance evaluation process involves cross comparisons among subjects' templates, as both probes and references, generated from biometric samples. Low-quality samples, even few in amount, can play a major role [17] in contribution to error rates, e.g., the false match rate (FMR) and the false non-match rate (FNMR). The purpose of sample quality control, i.e., trying to discern low-quality probe samples, is indispensable for a biometric system expected to operate in high accuracy.

To define the concept of biometric sample quality in a standard way, the international standard ISO/IEC 29794–1:2009 [10] considers it from three different perspectives:

- (1) Character, based on the inherent features of the source, e.g. poor character due to scars in a fingerprint;
- (2) Fidelity, reflecting the degree of a sample's similarity to its source;
- (3) Utility, indicating how (positively or negatively) a sample, by its quality status, contributes to the accuracy performance of a biometric system. Obviously the utility has dependency on both the character and the fidelity of a sample.

For a biometric recognition system, the utility of a sample is of most interest because it is directly contributing to the recognition accuracy. To describe fingerprint sample quality, normalized comparison score, expressed by NIST in Eq.(1) was defined in [9], which we believe can be generalized to all biometric modalities to characterize the utility of a biometric sample in the recognition accuracy sense expressed by error rates. Suppose x_i is a sample to be assessed in quality, its normalized comparison score $c(x_i)$ is

$$c(x_i) = \frac{s_m(x_i) - E[s_n(x_{ji})]}{\sigma(s_n(x_{ji}))} \quad (1)$$

where $E[\cdot]$ is a mathematical expectation, $\sigma[\cdot]$ is a standard deviation, $s_m(x_i)$ is a genuine comparison score generated by comparing the probe x_i to its reference originated from the same finger, and $s_n(x_{ji})$ are the imposter scores of sample x_i generated by comparing the probe x_i to the references originated from non-mated fingerprint samples, $\forall j, i \neq j$. Characterizing the distinguishability of the genuine comparison score from all imposter scores obtained from the studied probe

sample, the quality metric expressed by Eq.(1) goes coherently with the recognition performance in the sense of error rates. However, calculating a normalized comparison score implies comparisons between a probe and all references in the database. This process is unrealistic to launch as an online operation due to a high computational complexity, let alone when a sample is used for enrolment there does not exist any reference at all. These facts negate the feasibility using the normalized comparison score directly to assess a sample's quality. However, the normalized comparison score can be reasonably deemed as ground truth of the quality of a sample in the sense of utility, and thus provide a reference to correlation calculations (*e.g.*, Spearman's rank correlation [9]) with any quality metrics that can be operated in an online mode without requiring information provision from biometric references in the database. Such a recognition performance predictive approach suitable for online operation is what we called sample quality assessment approach in this paper.

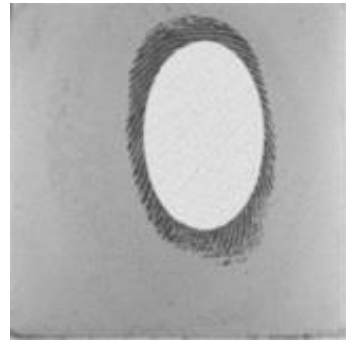
In the case of fingerprint samples, poor-quality samples generally produce spurious minutiae or lose genuine minutiae. For instance, a sample with partial fingerprint area captured can have only a small portion of minutiae recorded and even lose singular points (the core point and the delta point), which are important global reference points for sample alignment. For dedicated fingerprint sensors, in addition to partial fingerprint recording, low quality can be attributed to varying temperature / humidity conditions of the finger skin, low physical pressure, too less presentation time, incorrect finger positioning angles, *etc.* Such low-quality samples should be rejected after the sample quality assessment process, and a re-capturing action under improved environmental conditions should be initiated.

Clarity of ridges and valleys is a commonly recognized criterion to measure the quality of a fingerprint sample [13]. Several factors can influence the clarity of ridges and valleys, such as the acquisition sensor itself, the capturing environment, skin disease, skin humidity and specifically for touch-based fingerprint sensors also the pressure [12]. For example, a wet finger placed on an optical fingerprint sensor or high pressure exerted during a capture process will generate a sample image with connected dark area inside which ridges and valleys are difficult to discriminate. In some scenarios, fingerprint samples can be captured in a controlled environment compliant to standards [3; 10; 16; 17] to maximize the sample quality. For example, automatic fingerprint identification systems (AFIS) are widely deployed for border control and other national and international identity management purposes, such as the Visa Information System (VIS) in Europe, US-VISIT / IDENT system in US, and the Aadhaar project in India. In such scenarios, professional sensors distinguished from massive performance tests are usually chosen to acquire fingerprint samples under an ideal environment (fair and stable illumination, comfortable indoor climate, assistance and guidance from attendants, *etc.*).

As mentioned in Section 1, numerous fingerprint sample quality assessment methods [9; 11; 12; 13; 14; 15; 18; 19; 20] have been proposed using various quality features for sample

quality assessment. Some of the quality features have been incorporated into the ISO/IEC technical report [16]. As a holistic approach employing multiple features (including minutiae) and artificial neural network for fingerprint sample quality assessment, the NFIQ function [9; 21] was released by NIST in 2004 and widely adopted since. The NFIQ function can label a sample in 5 quality levels among which level 1 indicates the best quality. Since the year 2011, the NFIQ2.0 project [22], as an improved version of NFIQ, has been initialized and is currently under progress. However, all these methods mentioned above focused on samples captured by traditional sensors and did not consider the characteristics of smartphone-camera fingerprint samples.

B. What makes smartphone camera based fingerprint capturing different



(a) Captured by optical sensor L-1 DFR2100



(b) Captured by camera embedded in Samsung Galaxy S

Fig. 2. Two samples from the same finger (the fingerprint in (a) is cropped for privacy protection purpose in this example)

In consumer markets, Apple has released iPhone 5s with a fingerprint sensor built into the phone's home button [6]. Although such integrated dedicated fingerprint sensors can better ensure the sample quality, they incur additional cost and space occupation in a smartphone. The cameras embedded in smartphones, however, are promising to provide us an alternative option to sense fingerprint at almost no hardware cost. Such touchless sensors can in theory generate samples in higher utility compared to touch-based sensors because they can capture a larger finger area, which translates to more distinguishable features (*e.g.*, more minutiae) [23]. Nowadays a typical smartphone is equipped with a high-resolution 5~20 mega-pixel camera, which enables them to capture fingerprint

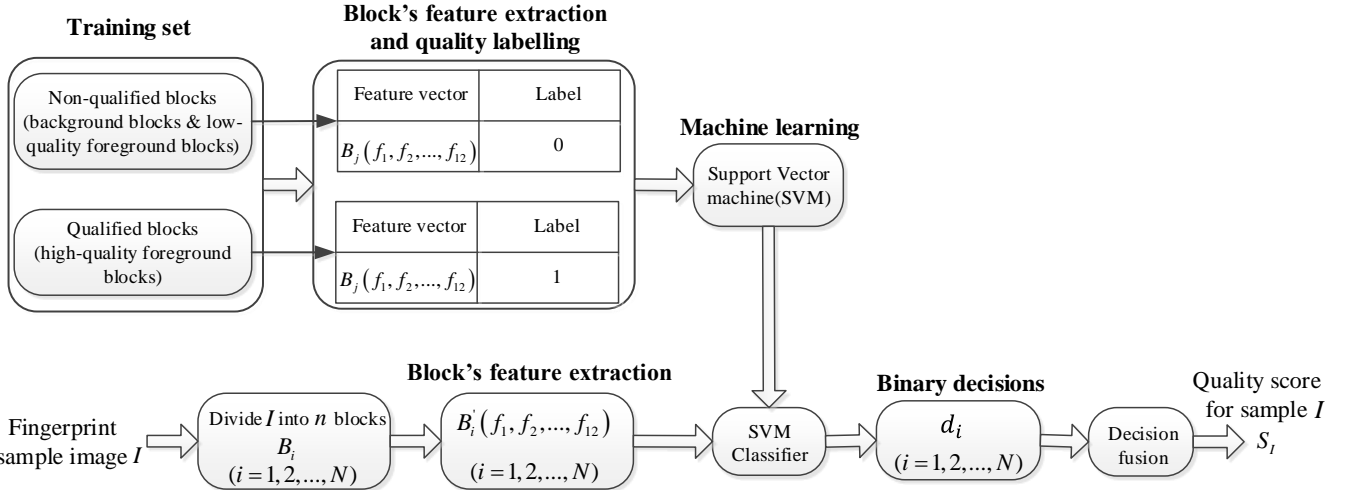


Fig. 5. The proposed one-stop-shop sample quality assessment approach

samples equivalent to very high DPI (dots per inch). Previous research [5; 24; 25] have shown this possibility.

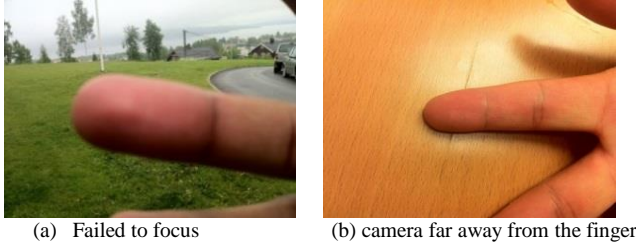


Fig. 3. Two samples captured by a smartphone camera: (a) failed to focus; (b) camera was too far from the finger

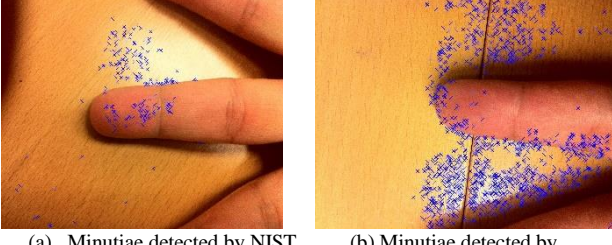


Fig. 4. Samples with high quality (level 1) labelled by NFIQ: blue cross marking the detected minutiae

Compared to the case fingerprints are captured by a general-purposed camera in an ideal laboratory environment [5; 24; 25], the samples captured in real life scenarios defined in our previous work [26; 27; 28; 29] show quite unstable quality due to camera motion, de-focusing, unfavored illumination, incorrect finger positioning, and complicated backgrounds. Fig. 2 illustrates two fingerprint samples captured from the same finger: Fig. 2(a) is a sample captured by a touch-based optical sensor L-1 DFR2100 and Fig. 2(b) is a sample captured from the same finger by the camera embedded in Samsung Galaxy S. Fig. 3 shows two smartphone camera fingerprint samples which are not qualified for the recognition purpose: (a) fails to focus on the finger area; and in (b) the camera was placed too far resulting in low resolution in the fingerprint area. In both samples, the ridges and valleys are not able to record and thus

impossible for feature extraction required for recognition. Such samples should be precisely detected by a sample quality assessment function and then discarded.

Observed from Fig. 2 we can see the difference between the two types of samples: samples captured from traditional fingerprint sensors (including those professional touchless fingerprint sensors such as TST BiRD [30]) exhibit relatively stable quality characterized by clean and homogeneous background, evenly distributed illumination, fair focusing and positioning, but limited fingerprint area; while samples captured from smartphone cameras exhibit unstable quality characterized by unpredictable background, sometimes biased illumination and de-focusing, but in general larger fingerprint area.

As mentioned in Section 2.1, there exist many quality assessment approaches for samples captured like the type in Fig. 2(a). But it is doubtful such methods can be directly applied to those smartphone camera fingerprint samples like the type in Fig. 2(b), assuming that complicate foreground segmentation and illumination adjustment required by such smartphone-camera samples have never been incorporated into the design of traditional quality assessment approaches. To verify this assumption, we tested the NFIQ function on some smartphone camera samples and only found that a significant percentage of samples labelled with high quality (level 1) are in fact low-quality ones. As minutiae count and quality information are used in NFIQ, these challenging samples might fool the NFIQ function with too many spurious minutiae detected from both the background and foreground. Fig. 4 illustrates two examples in this case, where (a) and (b) show minutiae detection results by the NIST function MINDTCT and the widely-used commercial minutiae detector Neurotechnology VeriFinger 6.0 Extractor [31], indicating both these two popular minutiae detectors were not good at coping with such smartphone-camera fingerprint samples. From these observations, we can reasonably infer that simple pre-processing mechanisms (e.g., the quality map used in NFIQ to identify foreground blocks) are not capable towards such samples.

C. One-stop-shop quality assessment

The spurious minutiae detection in the examples in Fig. 4 is due to lack (or incapability) of accurate foreground segmentation. An accurate segmentation algorithm usually requires intensive computation. Such intensive resource consumption could be unsuitable for the iterative process of quality control shown in Fig. 1, especially for mobile devices. In addition, such an accurate segmentation algorithm itself is not easy to achieve dealing with unpredictable backgrounds. Furthermore, unlike traditional fingerprints, which are evenly illuminated under a controlled environment, a lot of samples captured by smartphone cameras are biasedly illuminated causing shade areas within a finger area, such as the typical case in Fig. 3(a). Such shades are easy to detect as foreground but actually provides no useful information for recognition. Considering all these facts, we envision a segmentation-free approach that discriminates high-quality fingerprint patterns from those low-quality ones and the background ones in one operation. We propose in this paper such a one-stop-shop quality assessment approach for smartphone-camera fingerprint samples in real-life scenarios. Details are given in Section 3.

III. PROPOSED QUALITY METRICS

A. Pipeline of the proposed approach

The proposed one-stop-shop approach, as shown in Fig. 5, divides a sample image I into N non-overlapping blocks B_i ($i = 1, 2, \dots, N$), and checks each image block's quality status - qualified or non-qualified (including the low-quality case and the background case) - before fusing all blocks' quality decisions d_i to produce the final quality score S_I for the sample. From each block, a 12-dimensional quality feature vector B_i (f_1, f_2, \dots, f_{12}) is formed. During enrolment, such quality feature vectors together with their ground-truth quality labels are used to train a SVM classifier; and during quality assessment, a probe sample is labelled by the trained SVM classifier as “qualified” or “non-qualified”. The ground-truth blocks are selected and labelled manually according to their sources, i.e., samples with low and high normalized comparison scores. Summation is selected as the decision fusion rule. In this way, $\#QB$, the number of “qualified blocks” in a sample can be output as the quality score S_I after being normalized by the number of blocks in the sample:

$$S_I = \frac{\#QB}{N} \quad (2)$$

During the sample capturing process, the subject can be required to place his/her finger in an appropriate finger-to-camera distance. A simple rule, used in photography for sharpness evaluation [32], is to evenly divide the whole image into 3×3 rectangular regions and require the foreground (fingerprint area) to approximately cover this central region. In addition, to offset the variability in digital resolution of different camera settings, we define the block size in a way that in average around 4~10 ridges can be identified in one block. Heuristically, the block size (in pixel amount) can be determined against the size of the central region.

B. Block orientation alignment

Before feature extraction, all blocks need be aligned in orientation, assuming a high-quality block contains

homogeneously-oriented ridges. If the block size is large (e.g., ridge count > 10), this assumption may not apply to those extremely-high curvature ridge areas, e.g., the core or delta points. Fortunately, such areas normally cover only a small percentage of an entire fingerprint. Besides, the typical block size of 4~10 ridges limits the inhomogeneity in orientation. We tested a subset of blocks from our test database and found only $< 4\%$ blocks have challenge in orientation alignment, judged by human eyes, among which except those inherently high-curvature blocks, most inaccurate orientation alignment have only distortions of 5~10 degrees.

Suppose an image block B_i is sized $R \times C$ in pixel (R and $C = 2^k, k = 1, 2, 3, \dots$). After low-pass Gaussian filtering to suppress random noises, the Principal Component Analysis (PCA) based gradient orientation estimation method [33] is used to find a block's principal orientation. That is, inside each block neighboring pixels' differences d_v and d_h (in vertical and horizontal directions respectively) are obtained to form a gradient vector with orientation $\tan^{-1}(d_v/d_h)$. Then the block principal orientation θ_i is calculated by PCA to identify the principal one among all orientations of the $(R - 1) \times (C - 1)$ calculated gradient vectors. By clock-wisely rotating the $\sqrt{2}(R - 1) \times \sqrt{2}(C - 1)$ size area concentric to B_i by angle θ_i , we can crop a block B'_i sized $R \times C$ concentric to B_i . In this way we assume B'_i has the maximum gradient in the horizontal direction. Note that this block principal orientation derived from gradients is perpendicular to the principle orientation of the block ridges.

C. An efficient ridge pattern descriptor – Differential-Autocorrelative-Integration (DAI)

After block orientation alignment, quality features can be extracted from the ridge pattern. Assuming that a fingerprint ridge block exhibits a periodic characteristic that can be approximated by sinusoidal-wave-like ridge and valley repetition, we expect to represent this periodic characteristic by spatial frequency (called “principal frequency” in Section 3.4.) while suppressing noises in other frequency bands. Driven by this intuition, we propose the following procedure to describe a block ridge pattern.

Step 1 Differential operation along rows. With low-pass filtering done before orientation alignment, we consider using differential operation, effecting as high-pass filtering to capture the ridge-valley variations, on neighboring pixels along each row in the orientation aligned block B'_i . It is an operation same as we performed on B_i to calculate d_h during orientation alignment.

Step 2 Autocorrelation along rows. Autocorrelation [34], as a commonly-used signal processing method to detect periodic patterns polluted by noises, is used on the $(C - 1)$ pixel residues in each row. After the autocorrelation calculation, we keep the former $(C - 1)$ dimensions and remove the latter $(C - 2)$ redundant dimensions of the autocorrelation result vector

Step 3 Integration along columns. Sum up all R autocorrelation results to obtain a $(C - 1)$ dimensional vector. Here summation is used to increase the robustness of the descriptor by suppressing, if any, local minor

inhomogeneity in ridge pattern (e.g., caused by ridge endings and bifurcations).

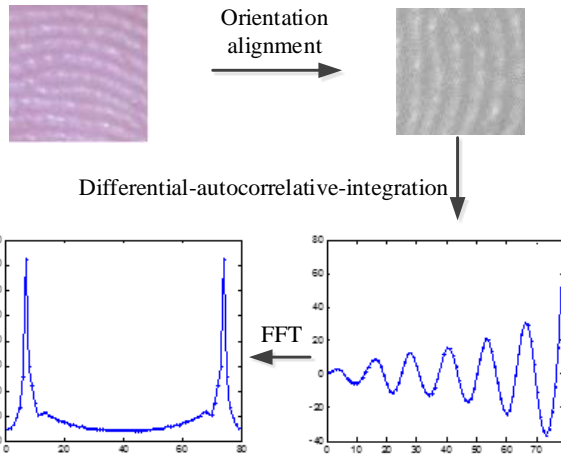


Fig. 6. Processing a high-quality block

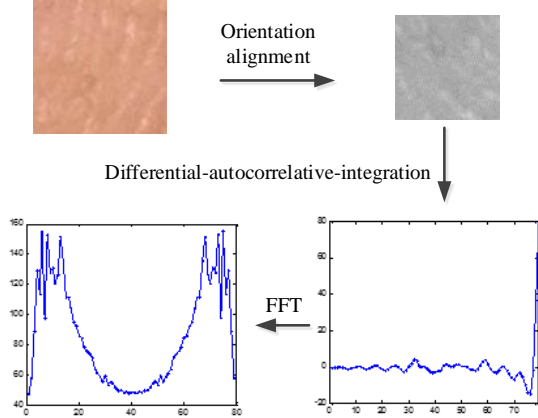


Fig. 7. Processing a low-quality block

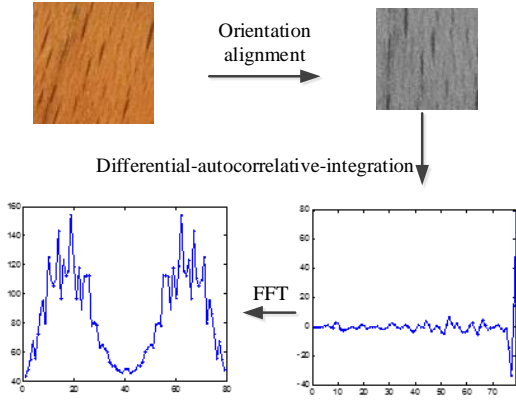


Fig. 8. Processing a ridge-like background block

We name the above three-step operation as Differential-Autocorrelative-Integration (DAI), as a new ridge pattern descriptor for quality feature extraction. Both spatial domain and Fast Fourier Transformation (FFT) frequency domain features can be extracted from this DAI descriptor, as we show in Section 3.4.

As we can observe from Fig.6-8, for a high-quality block, the absolute amplitudes of local peaks and valleys take on a stable increase in Fig. 6. However this cannot be observed for a low-quality block and a background block as shown in Fig. 7 and Fig. 8. Moreover, in the Fourier transform domain we can observe the highest peak has distinctly higher prominence in a high-quality block as seen in Fig. 6.

D. Proposed quality features

We summarize the description of Section 3.1-3.3 and illustrate the proposed sample quality assessment pipeline in Fig. 9.

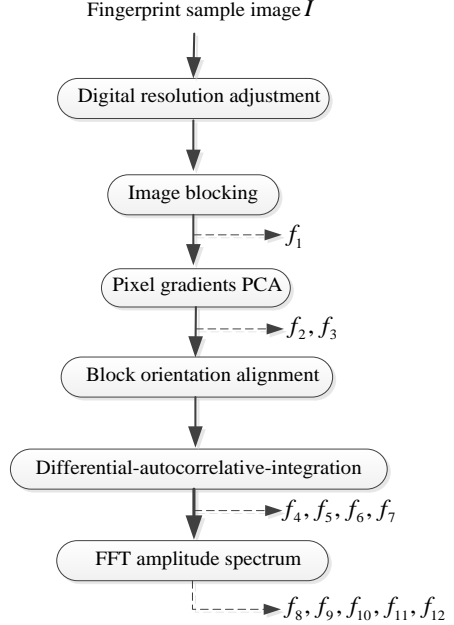


Fig. 9. Features extraction from different steps of the proposed pipeline

We propose 12 quality features $f_i (i = 1, 2, \dots, 12)$ of three types to assess an image block's quality: (a) 3 pixel based features; (b) 4 DAI descriptor based features; c) 5 spectrum features of the DAI descriptor. A quality feature vector can be formed by these 12 features for an image block. The detail of each feature is described as follows. Note that these 12 features are not necessarily in practice the best ones for smartphone camera fingerprint sample quality assessment but included in order to characterize the different dimensions of fingerprint patterns.

i). Pixel based features

- (1) f_1 : Exposure, calculated from the average pixel value of B_i

$$f_1 = \frac{1}{R \times C} \sum_{r=1}^R \sum_{c=1}^C B_i(r, c) \quad (3)$$

where $B_i(r, c)$ is the pixel at the r -th row and c -th column inside the block B_i . Both too-bright and too-dark fingerprint areas are unfavored for feature extraction.

- (2) f_2 :

$$f_2 = \lambda_1 \quad (4)$$

where λ_1 is the first eigenvalue of the covariance matrix of all gradient vectors obtained from the PCA calculation, indicating the significance of a block's principal orientation calculated in Section 3.2.

- (3) f_3 : Certainty of the principal orientation. We use a modified definition of ocl (orientation certainty level) in [16] as follows:

$$f_3 = \begin{cases} 1 - \frac{\lambda_2}{\lambda_1} & \text{if } \lambda_1 \neq 0 \\ 0 & \text{if } \lambda_1 = 0 \end{cases} \quad (5)$$

where λ_2 is the second eigenvalue of the covariance matrix of all gradient vectors.

ii). DAI descriptor based features

As described in Section 3.3., we calculate autocorrelation on the horizontally-differential vectors $\mathbf{d}_i(r), 1 \leq r \leq R-1$, and obtain the DAI descriptor as

$$\mathbf{DAI}_i = \sum_{r=1}^{R-1} \text{autocorr}(\mathbf{d}_i(r)) \quad (6)$$

where, $\mathbf{d}_i(r) = (b_i(r, 2) - b_i(r, 1), b_i(r, 3) - b_i(r, 2), \dots, b_i(r, C) - b_i(r, C-1))$, and

$\text{autocorr}(\mathbf{d}_i(r))(j) = \sum_{c=1}^{1+j} \mathbf{d}_i(r, c) \mathbf{d}_i(r, C-2+c-j)$, ($0 \leq j \leq C-2$), with all $(C-1)$ amplitudes divided by the highest amplitude of $\text{autocorr}(\mathbf{d}_i(r))$. Before the subsequent feature extraction steps, a low-pass filtering is applied by setting the upper half of \mathbf{DAI}_i 's DCT-transform frequency coefficients to zero. Thus a smoothening of the \mathbf{DAI}_i vector is reached, denoted as \mathbf{ACR}_i .

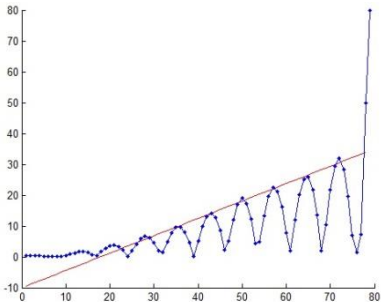


Fig. 10. $|\mathbf{ACR}_i|$ curve (i.e., the absolute amplitudes of first half of \mathbf{DAI}_i 's autocorrelation), $C = 80$ (the straight line is the linear best fit of the M peak points)

- (4) f_4 : $|\mathbf{ACR}_i|$'s peak activity rate.

From the observation in the experiments, we find the local peaks (excluding the maximum peak i.e. the $(C-1)$ th dimension of \mathbf{ACR}_i) of the $|\mathbf{ACR}_i|$ curve (i.e., the absolute amplitude curve of \mathbf{ACR}_i) have a stable increasing rate in those ground-truth good quality blocks. We use a 1st-order polynomial (i.e. a straight line) to fit the M detected peaks in their x-coordinates $x_{p1}, x_{p2}, \dots, x_{pM}$ in the $|\mathbf{ACR}_i|$ curve (shown in Fig. 10) and obtain a fitted straight line with slope value S. M amplitudes $A(x_{pn}) (n = 1, 2, \dots, M)$ on the fitted line can be found. Then the $|\mathbf{ACR}_i|$'s peak activity rate is defined as:

$$f_4 = \frac{1}{M} \sum_{n=1}^M A(x_{pn})(A(x_{pn}) > 0) \quad (7)$$

As we can observe in Fig. 6 and Fig. 7, the peaks in the autocorrelation result are closer to the x-axis for low-quality blocks and background block than the high-quality block case. Thus the value of f_4 is expected to be significantly higher for a high-quality block.

- (5) f_5 : $|\mathbf{ACR}_i|$'s peak pick-up rate.

We denote it using the slope of the straight line in Fig. 9. A denotes the amplitudes (y-coordinates) in x-coordinates x_{pn} on the line:

$$f_5 = S = \frac{A(x_{p(n+1)}) - A(x_{pn})}{x_{p(n+1)} - x_{pn}} \quad (8)$$

where $n \in 1, 2, \dots, M$. This feature may take on a high value if the ridges in the block are not uniformly illuminated or influenced by external noises like dirt spots.

- (6) f_6 : $|\mathbf{ACR}_i|$'s peak variance rate.

We use this rate to represent the degree that the actual M peak amplitudes $y_{p1}, y_{p2}, \dots, y_{pM}$ deviate from the fitted line.

$$f_6 = 1 - \frac{\sum_{n=1}^M |y_{pn} - A(x_{pn})| / M}{\max(A(x_{pn})) - \min(A(x_{pn}))} \quad (9)$$

where $n \in 1, 2, \dots, M$. This feature may take on a high value if the ridges in the block are not uniformly illuminated or influenced by external noises like dirt spots.

- (7) f_7 : $|\mathbf{ACR}_i|$'s peak drop rate.

We use this rate to represent the degree of the amplitude drop $AD_n = y_{p(n+1)} - y_{pn} (n = 1, 2, \dots, M-1)$ of one peak compared to its neighboring peak on the left side. From the observation in the experiments, large drops in amplitude seldom happen to high quality blocks.

$$f_7 = 1 - \frac{(\sum_{n=1}^{M-1} |AD_n| / (M-1))}{\max(A(x_{pn})) - \min(A(x_{pn}))} \quad (10)$$

iii). Spectrum feature of the DAI descriptor

This type of features is derived from the FFT amplitude spectrum characteristics of \mathbf{ACR}_i , which we denote as $|f\mathbf{ACR}_i|$, characterizing ridges' spatial frequency properties.

- (8) f_8 : Principal frequency's amplitude:

$$f_8 = \max(|f\mathbf{ACR}_i|) \quad (11)$$

Due to the periodicity of ridge structures, a high-quality block may have a principal frequency with high amplitude in its FFT amplitude spectrum.

- (9) f_9 : Principal frequency, i.e., f_8 's frequency index in the amplitude spectrum.

As observed in Fig. 6 to Fig. 8, most of the energy concentrates on the principal amplitude and its neighbors in the high-quality blocks, forming a sharper peak. The features f_{10}, f_{11}, f_{12} are thus extracted to describe the degree of energy concentration. The feature f_{10} depicts the energy distribution among a quarter of $|f\mathbf{ACR}_i|$'s components with highest amplitudes. The feature f_{12} and f_{11} depict the energy distribution among a close adjacent and a second-close adjacent frequency ranges centering the principal one.

- (10) f_{10} : Principal frequency's dominance rate:

$$f_{10} = 1 - \frac{4 \times \sum_{n=2}^{C/4} Q_i(n)}{(C-4) \times Q_i(1)} \quad (12)$$

where we denote $Q_i(1), Q_i(2), \dots, Q_i([(C-1)/4])$ as the quarter of $|f\mathbf{ACR}_i|$'s highest amplitudes, i.e., the amplitudes of former $[(C-1)/4]$ frequencies of $f\mathbf{ACR}_i$ after being sorted in a descending order by amplitude. Obviously, $Q_i(1) = f_8$. A high value of feature f_{10} indicates good quality for a block, in the sense that the amplitude spectrum has a dominant principal frequency compared to its peer amplitude peaks, if any.

- (11) f_{11} : Principal frequency's prominence rate - close adjacent frequency range:

$$f_{11} = 1 - \frac{(\sum_{n=-H}^H F(L+n) - F(L))}{2H \times F(L)} \quad (13)$$

where L is the principal frequency's index in the amplitude spectrum vector $F = |f\mathbf{ACR}_i|$, $H > 0$, and $L - H > 0$, otherwise $f_{11} = 1$. We consider only the $2H$ -width adjacent

frequency range around the principal frequency. Here $F(L) = Q_i(1) = f_8$.

(12) f_{12} : Principal frequency's prominence rate - second-close adjacent frequency range:

$$f_{12} = 1 - \frac{\sum_{n=-X}^X F(L+n) - \sum_{n=-H}^H F(L+n)}{2(X-H) \times F(L)} \quad (14)$$

where L is the principal frequency's index in the amplitude spectrum vector $F = |f \mathbf{ACR}_i|$, $0 < H < X$, and $L - X > 0$, otherwise $f_{12} = 1$. A high value of feature f_{11} and f_{12} indicate good quality for a block, in the sense that the principal frequency's amplitude takes on a prominent peak outstanding from neighboring frequencies.

E. Feature dynamic range normalization

The features $f_i (i = 1, 2, \dots, 12)$ are z-score normalized prior to being used by the SVM:

$$f'_i = \frac{f_i - E(f_i)}{\sigma(f_i)} \quad (15)$$

where $E(\cdot)$ and $\sigma(\cdot)$ E

IV. EXPERIMENTAL SETTINGS

A. Experiments design and dataset collection

For evaluating a quality assessment approach, we assume that higher quality samples result in lower error rates in recognition performance testing. We can thus use the normalized comparison scores [9] as the ground truth to calibrate samples' quality by correlating the quality scores calculated from the proposed one-stop-shop approach with their normalized comparison scores. Three evaluation metrics - Spearman's rank correlation coefficient, Error versus Reject Curves (ERC) [14], and false detection rate - were adopted to evaluate the performance of the proposed quality assessment approach, with results given in Section 5.

Three smartphones: iPhone 4, Samsung Galaxy I, and Nokia N8 were used to capture fingerprint samples from 100 different finger instances from 25 subjects. From each subject, four fingers - left index, left middle, right index, and right middle - were required to generate 3 samples from each. Table I specifies the three smartphone cameras. We considered three real-life scenarios: (1) the indoor scenario with ideal illumination but a challenging background (desk surface) (Fig. 11(a)); (2) the dark scenario with only illumination from the smartphone's automatic flash (Fig. 11(b)); and (3) the outdoor scenario with a complicate background (Fig. 11(c)). All three smartphones were used in the indoor and the outdoor scenarios but only Nokia N8 was used in the dark scenario (the other two failed to capture samples in darkness). In total there are 2100 fingerprint samples captured.

TABLE I
SPECIFICATION OF THE THREE SMARTPHONES' CAMERAS

Mobile phone	Nokia N8	iPhone 4	Samsung Galaxy S
Mega pixel	12.0	5.0	5.0
Resolution	1536×1936	2592×1936	1600×960
Auto-focus	Yes	Yes	Yes
Image format	JPEG	JPEG	JPEG
ISO control	Automatic	Automatic	Automatic
Flash source	Xenon	LED	No flash
Flash setting	Automatic	Automatic	No flash
Aperture	f/2.8	f/2.8	f/2.6
Sensor size	1/1.83"	1/3.2"	1/3.6"

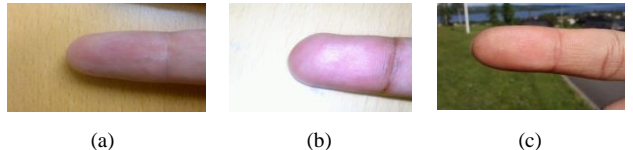


Fig. 11. Fingerprint samples captured in three scenarios: (a) indoor; (b) dark (automatic flashing); (c) outdoor

B. Pre-processing for ground-truth quality calculation

The proposed approach does not need to segment the foreground (finger area) for quality assessment. However, to obtain the normalized comparison scores as sample quality's ground truth, pre-processing is required to the captured samples to generate fingerprint templates. Such pre-processing steps could include (1) segmentation of the fingerprint area; (2) sample resizing (to offset the distance variance of fingers from the camera); and (3) fingerprint area enhancement.

Pre-processing step 1: manual segmentation is performed to crop the foreground as a ground-truth fingerprint area. In practical fingerprint recognition systems, a segmentation algorithm such as the pre-processing in [5] can be applied to for segmentation in real time. How to improve accuracy and efficiency of the pre-processing is key to recognition performance but out of scope of this paper.

Pre-processing step 2: Sample resizing is implemented by the following sub-steps: (1) fit the fingertip shape as a half-circle, and detect this circle using the Hough transform over the boundary of the foreground; (2) align the radius of the detected fingertip half-circle to a constant value; and (3) resize the whole cropped sample according to the new aligned radius. In this way, all the resized samples contain fingertips with almost the same radius. After the resizing, the fingerprint enhancement implementation from [35] is applied to enhance the ridge orientation and frequency.

Pre-processing step 3: Histogram equalization will be performed to enhance the sample output from the pre-processing step 2.

Note that all the pre-processing steps mentioned above are only for normalized comparison scores calculation instead of quality assessment in our proposed approach. In this paper, all the quality scores are generated from the full-size original samples with full backgrounds. We assume such a segmentation-free quality estimation step is efficient in computation and thus suitable for smartphones since an accurate segmentation algorithm usually requires intensive computations. Nevertheless, some suboptimal-but-efficient

segmentation [36] can be used prior to the proposed approach to further reduce the computational complexity.

C. Dataset preparation and parameter setting

We applied the aforementioned pre-processing steps to the 2100 samples and obtained a foreground-cropped dataset in order to calculate the normalized comparison scores as ground-truth sample quality. The VeriFinger 6.0 Extractor was used to generate the templates from this foreground-cropped dataset. There are only 906 foreground-cropped samples successful in generating templates, which should be attributed to VeriFinger's own sample quality control functionality. In order to create a training set, which covers sufficient high-quality blocks and non-high-quality ones, we selected 29 samples (high-quality ones by visual check) out of those original full samples that generated the 906 templates, and selected 21 samples (low-quality ones by visual check) from the rest 1194 ($= 2100 - 906$) original full samples. The two groups of selected samples were taken as SVM's training sets. The original captured 2100 fingerprint samples were thus divided into three datasets in our experiments:

Dataset_50 (training set): those original full fingerprint samples used for selecting blocks for SVM training, consisting of two sub-sets – the 29 high-quality samples and the 21 low-quality samples. Fig. 12 shows some examples of high-quality sample blocks, low quality ones, and background ones.

Dataset_877 (testing set I): there are 877 ($= 906 - 29$) fingerprint samples used for testing. The corresponding 877 foreground-cropped samples are able to generate templates by VeriFinger 6.0 Extractor. Thus we can calculate a normalized comparison score for each sample in this dataset.

Dataset_1173 (testing set II): there are 1173 ($= 1194 - 21$) fingerprint samples used for testing. The corresponding 1173 foreground-cropped samples are unable to generate templates by VeriFinger 6.0 Extractor. Thus we set their normalized comparison scores to zero in experiments.

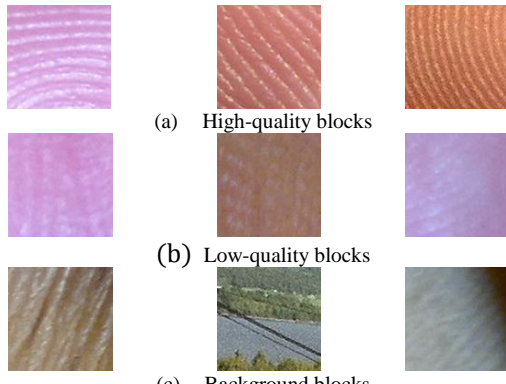


Fig.12. Examples of high-quality, low-quality, and background blocks from the training set Dataset_50. (the left and right blocks in (c) were from the background of the authors' wood-texture office desktop)

To align the digital resolution roughly equivalent to that of the other two cameras, we enlarged the samples generated by Samsung Galaxy S camera 1.5 times. Other parameters used in our experiments are listed in Table II. The block size $R = C = 80$ was heuristically set in order to meet the ridge density requirement of 4~10 ridges per block. Table III gives the statistics of image blocks used in the experiments.

**TABLE II
EXPERIMENTAL PARAMETER SETTINGS**

Parameter	Value
Scaling factor of training function	1
$R = C$	80
H	2
X	4
Training function 'kernel function' of 'svmtrain'	svmtrain in Matlab rbf

**TABLE III
STATISTICS OF SAMPLE BLOCKS USED IN THE EXPERIMENTS**

Dataset	Amount of block used
Training set	Dataset_50: sub-set_29
	Dataset_50: sub-set_21
Testing set	Dataset_877
	Dataset_1173

D. The distribution of quality features

It would be interesting to see the distribution of the proposed quality features calculated from the training set. The training set consists of 77 qualified blocks and 797 non-qualified blocks. We compute the feature vectors from the two sets of blocks respectively and give the result in Fig. 13. The light blue box indicates the qualified case and the dark blue box for the non-qualified case. In general, a good quality feature would be desired to maximize the separability of the two sets of blocks.

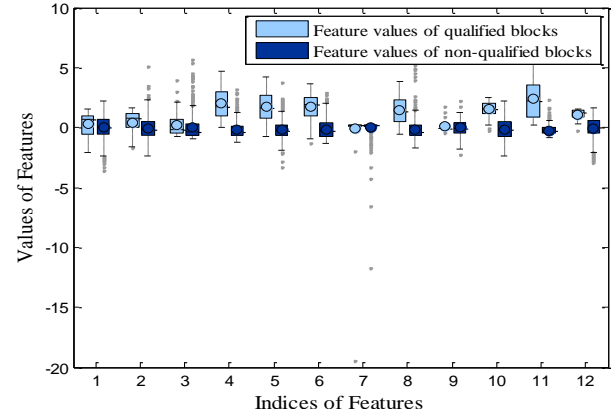


Fig.13. Quality feature value distribution

E. Quality scores generation

Our quality assessment approach addresses the full image without needing segmentation since it regards both low-quality blocks and background ones as non-qualified. We generate a quality score for each sample in Dataset_877 and Dataset_1173. Fig. 14 gives examples of qualified samples with qualified (high-quality foreground blocks) marked by white cross ('X') blocks.

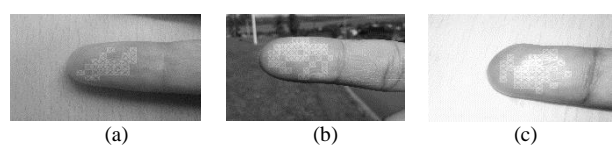


Fig. 14. Samples with high-quality foreground blocks detected in three scenarios: (a) indoor; (b) dark; (c) outdoor.

The quality score is calculated in this way: first we divide a sample's quality score (the amount of qualified blocks detected from the sample) by the number of the sample's blocks as mentioned in Section 2, and then normalize the division result to the dynamic range [0, 100]. The sample's quality score is expressed as

$$q_i = \frac{S_i - \min(S)}{\max(S) - \min(S)} \times 100 \quad (16)$$

where S_i is the quality score of the i th sample image in Dataset_877 or Dataset_1173, calculated by Eq.(2). S is the set of all sample quality scores.

F. Normalized comparison scores generation

In order to evaluate the performance of the proposed approach, we need to calculate the normalized comparison score c_i ($i = 1, 2, \dots, 877$) for the i th sample in Dataset_877 as its ground-truth quality.

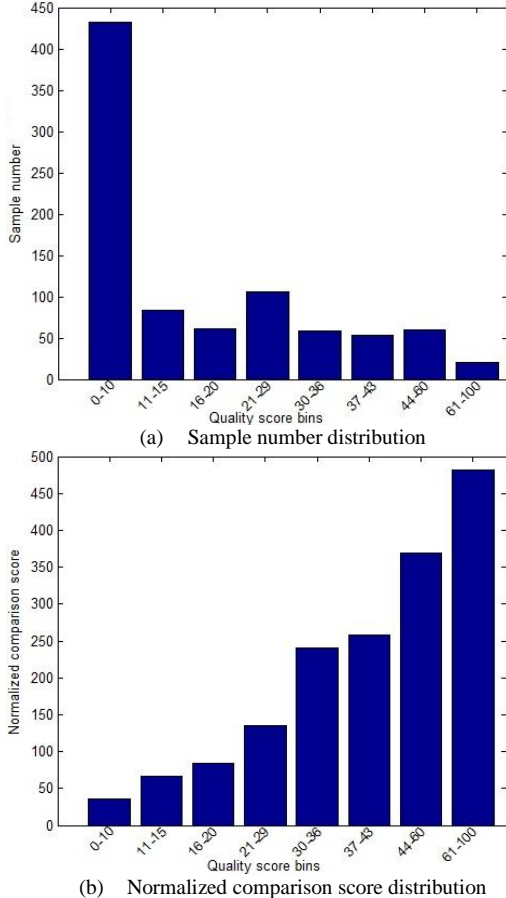


Fig. 15. Sample number and normalized comparison score distributions over quality score bins: Dataset_877 (which can generate templates by VeriFinger 6.0 Matcher)

We use the samples with the maximum quality scores calculated from the above sub-section as references in normalized comparison scores calculation by Eq.(1). VeriFinger 6.0 comparator was used to generate comparison score between two templates. To include these reference

samples themselves into quality assessment, we need to generate normalized comparison scores for them as well. Namely this requires a reference sample be compared to itself to obtain a genuine comparison score (i.e., $s_m(x_i)$ in Eq.(1)). We assign the globally highest genuine comparison score calculated from two different samples in the experiments to these reference samples as their genuine comparison scores. Fig. 15 presents the normalized comparison scores distributions over 8 quality score bins in Dataset_877. We can see good correlation between the quality scores and the normalized comparison scores from Fig. 15(b). The next section will quantitatively measure this observed correlation.

V. PERFORMANCE EVALUATION

In this section, we evaluate the performance of the proposed approach on two levels: the quality feature level and the holistic approach level. We suggest using three metrics to evaluate a quality assessment approach designed for smartphone camera fingerprint samples: Spearman's rank correlation, Error Reject Curves (ERC) and false detection rate. The three metrics can work in a complementary way focusing on different aspects of the evaluation.

On the quality feature level, we compare the proposed 12-dimensional feature vector with two standardized and widely-used local quality features, namely Local Clarity Score (LCS) [16] and Frequency Domain Analysis (FDA) [16]. For a fair comparison, when a sample quality score is calculated using LCS or FDA, the same pipeline procedures from "Digital resolution adjustment" to "Block orientation alignment" in Fig. 9 and the same scoring rule as in Eq.(16) are employed but to replace the proposed 12-dimensional feature vector based SVM decision by a thresholded LCS or FDA score decision for each block. For comparison, we also calculated the correlation coefficient by only using the f_{12} in the proposed pipeline by a thresholded f_{12} score decision.

On the holistic approach level, as it is difficult to find in publicized literature such a holistic approach targeted at smartphone-camera fingerprint samples, we can only compare the proposed approach as a whole to the NIST fingerprint sample quality assessment function NFIQ (described in Section 2), as it has been most widely used since being proposed.

A. Spearman's rank correlation

TABLE IV
SAMPLE QUALITY ASSESSMENT METHODS COMPARISON BY SPEARMAN'S RANK CORRELATION COEFFICIENT

Quality assessment method	Spearman's rank correlation coefficient ρ	
	Dataset_877	Dataset_877 + Dataset_1173
NFIQ	-0.0926	-0.0459
LCS in the proposed pipeline	0.4557	0.4172
FDA in the proposed pipeline	0.5490	0.4266
Only using 12 th feature in the proposed pipeline	0.4538	0.4412
Proposed approach	0.6086	0.5851

Computing the Spearman's rank correlation coefficient ρ ($-1 \leq \rho \leq 1$) is a quantitative method to analyze how well two variables correlate. A value of 1 or -1 indicates being perfectly monotonically correlated, while 0 indicates being uncorrelated. We compute the Spearman's rank correlation coefficient ρ between the normalized comparison score c_i and the quality score q_i generated by the proposed approach, over the two datasets Dataset_877 (testing set that can generate fingerprint templates by VeriFinger 6.0 Extractor) and {Dataset_877 + Dataset_1173} (all samples for testing). The results are given in Table IV. Note that for all quality scores generated we used original full samples without any segmentation. The results show that the proposed quality assessment approach can accurately predict a sample's quality in terms of higher correlation coefficients compared to NFIQ and the other two features (LCS and FDA) based approaches. We can see NFIQ missed the point completely when being used to assess such smartphone-camera fingerprint samples with complicate illumination and background. The result goes coherently with the analysis in Section 2.2, i.e., as an effective quality indicator to traditional fingerprint samples, NFIQ was not intended for such smartphone camera fingerprint samples. Compared to LCS and FDA in the same block-based quality assessment pipeline, the proposed 12-dimensional feature vector with SVM classification shows better performance too. To compare individual features, we achieved the correlation performance from f_{12} equivalent to LCS and FDA.

B. Reject Curves (ERC Error)

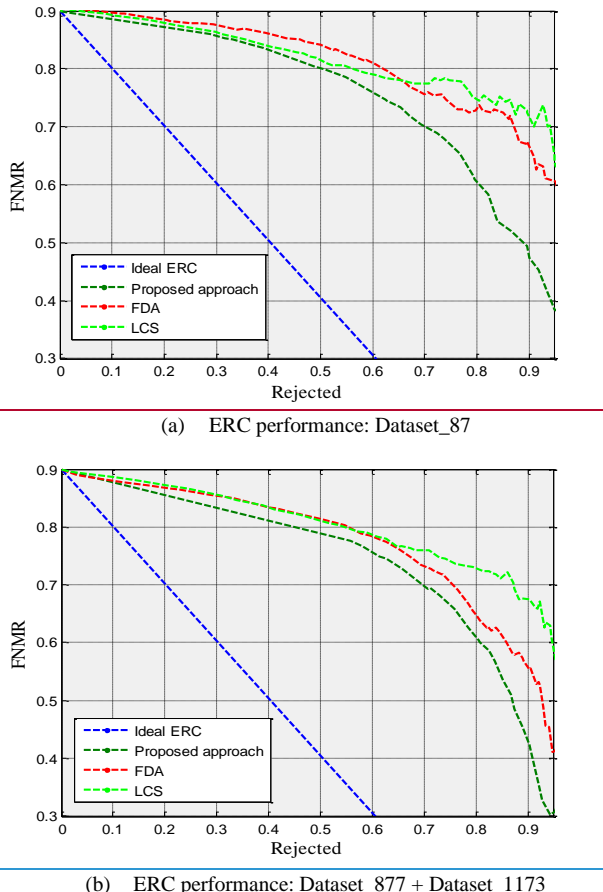


Fig. 16. Quality assessment methods comparison by error reject curves

Spearman's rank correlation is an efficient way to evaluate the correlation of two variables in a global sense. However, it does not give information how one variable can influence the other in a scalable way. For sample quality control in an operational mode, people may be interested in knowing how to find a suitable threshold for quality control to filter out some low-utility samples in order to achieve better system recognition performance, as a system's error rates (false match rate and false non-match rate) are usually contributed by a few low-utility samples [9]. Error reject curves (ERC) was proposed [14] to address this need to show how quality score threshold tuning (rejecting genuine comparison cases below the quality threshold) can influence the system's false non-match rate (FNMR). Each genuine comparison is assigned a quality score by Eq.(7) in the paper [14], which in our experiment equals to the lower one of the two samples' quality scores. An easy-to-understand way to the ERC metric is - suppose at a certain genuine comparison score threshold we have the a FNMR value, we can expect to reduce this FNMR by rejecting some percentage of the genuine comparison cases (both two samples associated with each comparison) with the lowest quality scores among all. In this sense, the correlation between the FNMR and the quality rejecting percentage can be measured in fine granularity. Fig. 16 compares the ERC performance of LCS, FDA, and the proposed approach over the two datasets Dataset_877 and {Dataset_877 + Dataset_1173}. We can see over both datasets the proposed approach excels the other two features based approaches. Here the same pipeline as the proposed approach was used for the two features. The FNMR was initialized at 90% just because this 2100-sample database is very challenging in sample quality in overall.

NFIQ performance was not illustrated in the ERC charts because of its apparently bad performance and sparse quality levels that are difficult to generate a curve.

C. False detection rate

TABLE V
COMPARISON OF FALSE DETECTION RATE (#FALSELY DETECTED BLOCK / # ALL DETECTED BLOCKS)

Quality metrics	False detection rate		
	Dateset_877	Dateset_1173	Dateset_877 + Dateset_1173
LCS in the proposed pipeline	69.85%	90.64%	78.4%
FDA in the proposed pipeline	80.56%	94.9%	86.74%
Only using the proposed 12 th feature in the proposed pipeline	12.89%	20.26%	16.16%
Proposed approach	2.67%	11%	4.02%

In our experiments, some samples are susceptible to false detection problem (background blocks labelled as high-quality ones), which mostly occurs in the indoor scenario with the challenging background - the authors' wood-texture office desk surface (shown in Fig. 3 and Fig. 4). Such false detection problem may not pose a direct threat to quality assessment if both the foreground and the background are well focused like the examples in Fig. 17. Fortunately, in our database, most of

such samples with challenging background have fair focus on the foreground at the same time, which leads to high correlation between the amount of false detected blocks and the amount of the qualified blocks on the foreground. This fact to some degree suppresses the influence of false detection to Spearman's rank correlation and the ERC performance in this testing database. However, we can envision for some untypical cases, such as no finger is captured in a sample with such challenging background, or the case the background instead of the foreground is focused, false detection will severely impact the performance of a quality assessment approach.

Table V lists the statistics of false detection under the four block-based quality assessment approaches. We can see the proposed holistic approach performs distinctly better than the same quality assessment pipeline adopting the other two features. On the individual quality feature level, f_{12} exhibits much lower false detection rate than LCA and FDA as well.

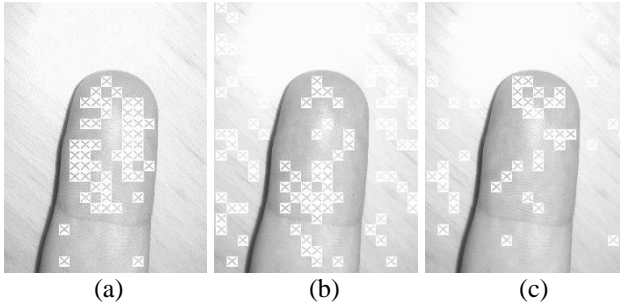


Fig. 17. False detection sample for three quality metrics: proposed approach, (b) FDA, and (c) LCS. Qualified blocks marked by cross.

D. Correlation between individual features and the block quality decision

We also evaluated the correlation between each of 12 features and the binary quality decision for each block by computing Spearman's rank correlation coefficient on Dataset_877. There are 418,430 blocks in Dataset_877 as listed in Table III. Thus 418,430 values for each feature can be computed, meanwhile 418,430 binary decisions can be produced by the SVM classifier. The Spearman's rank correlation can be calculated for the two sets of data. Table VI shows the correlation results for each feature on Dataset_877. We can see the DAI descriptor based features have stronger correlation with the binary decision comparing to the pixel based features.

TABLE VI

CORRELATION BETWEEN FEATURES AND BLOCK QUALITY DECISION CALCULATED ON DATASET_877

Features	f_1	f_2	f_3	f_4	f_5	f_6
ρ	0.046	0.005	0.038	0.22	0.22	0.20
Features	f_7	f_8	f_9	f_{10}	f_{11}	f_{12}
ρ	0.20	0.20	0.13	0.19	0.20	0.26

TABLE VII

EERs ON LEVELLED QUALITY SCORE GROUPS

	Group 1	Group 2	Group 3
Quality score	0-6	7-24	25-100
Samples number	375	264	238
Number of genuine scores	287	181	161

Number of imposter scores	22960	11765	10626
EER	25.6%	20.9%	6.8%

E. Purpose verification of quality assessment: EER under different levels of quality scores

Recall that the purpose of sample quality assessment is to select high quality samples for recognition use. To verify whether this purpose is achieved by the proposed approach or not, we calculate EERs under three levels of quality scores using VeriFinger 6.0 comparator. The sample with maximum quality score is always selected as the reference sample for each finger in all experiments. We divided the quality score range [0, 100] into three sub-ranges: [0, 14], [15, 33], and [34, 100] for the testing set Dataset_877. The experimental results are given in Table VII. We observe that EERs are significantly reduced along the increase of sample quality, which demonstrates the effectiveness of our proposed quality assessment approach in predicting the quality of fingerprint samples generated by the three smartphone cameras used in our experiments.

VI. CONCLUSIONS AND FUTURE WORK

To evaluate the quality of a fingerprint sample captured by a smartphone camera, we proposed an effective quality assessment approach, which processes a captured fingerprint sample by a block-based feature extraction pipeline. An accurate block ridge pattern descriptor – Differential-Autocorrelative-Integration (DAI) – was proposed for extracting quality features from each image block. In total 12 quality features in three types, namely pixel-based, DAI based, and DAI spectrum based, are extracted from each image block to form a 12-dimensional quality feature vector. SVM is trained and used to make a binary decision “qualified” or “non-qualified” for each feature vector. In addition, a 2100-sample smartphone camera fingerprint database is created to test the proposed approach.

In addition to better correlation with the ground-truth sample quality and lower block false detection rate, our approach differs from existing fingerprint quality assessment approaches in the following aspects:

- (1) The proposed approach directly detects high-quality foreground blocks and discards those low-quality foreground blocks and background blocks, therefore needing no segmentation of the foreground in advance. We call it a ‘one-stop-shop’ approach in this sense. This could be favored by mobile devices with constrained computation resources since accurate segmentation against complicate backgrounds usually requires intensive computation or performs unstably under varied illumination or backgrounds. Nevertheless, the proposed approach can work in harmony with an accurate and stable pre-segmentation algorithm if any;
- (2) The sample processing pipeline proposed in this paper, including the block orientation alignment, block-based quality feature vector generation, block-based SVM classifier, and the scoring rule for a sample, is structured in a way that the different processing steps can be easily maintained. This makes the proposed approach in essence

open to any improvement in performance. For instance, new quality features proposed in the future can be easily plugged into the pipeline for performance testing. We had already done this to two standardized features (LCS and FDA) in this paper.

Note that the 12 quality features proposed in this paper should not be deemed as the best ones for the purpose of smartphone camera fingerprint sample quality assessment. We adopt them only for characterizing a block pattern from different quality-related aspects.

Though targeting at smartphone camera fingerprint samples, the proposed approach can be reasonably generalized to other biometric system using touchless fingerprint sensors requiring effective and efficient sample quality control in unpredictable working environments, such as portable touchless fingerprint identification terminals used by law enforcement staffs.

Moreover, we studied the characteristics of smartphone camera fingerprint samples, explained why traditional approaches are incapable towards such samples, and verified these explanations by experimental results. Accordingly, three performance evaluation metrics for quality assessment on smartphone camera fingerprint samples were suggested based on their complementary focuses.

Future work is planned in the following aspects:

- (1) Real-time sample quality assessment from a smartphone's preview video sequence will be investigated;
- (2) New efficient quality features, especially features to qualify high-curvature blocks;
- (3) For better user convenience, methods for automatic resolution alignment and interactive focusing will be integrated.

REFERENCES

- [1] A.K. Jain, P. Flynn, A.A. Ross. (2007). "Handbook of biometrics". Springer.
- [2] ICAO. 2006. "Machine readable travel documents, ICAO Technical report."
- [3] ISO/IEC 19794–4. 2011. Information technology – biometric data interchange formats – part 4: finger image data.
- [4] ISO/IEC 19794–2. 2011. Information technology – biometric data interchange formats – part 2: finger minutiae data.
- [5] C. Stein, C. Nickel, C. Busch. (2012, September). "Fingerphoto recognition with smartphone cameras". In Biometrics Special Interest Group (BIOSIG), 2012 BIOSIG-Proceedings of the International Conference of the (pp. 1-12). IEEE.
- [6] Iphone fingerprint sensor. Accessed: 2014-05-03. <http://www.apple.com/iphone-5s/>.
- [7] MobbKey remote secure access control by biometrics and smartphone. Accessed: 2014-05-03. <http://www.mobbeel.com/products/mobbkey/overview/>.
- [8] FIDO identity authentication, Accessed: 2014-05-03. <https://fidoalliance.org/>.
- [9] E. Tabassi, C.L. Wilson, C. Watson. (2004). "Nist fingerprint image quality". NIST Res. Rep. NISTIR7151.
- [10] ISO/IEC 29794–1. 2009. Information technology – biometric sample quality – Part 1: framework.
- [11] A. Fernando, J. Fierrez, J. Ortega-Garcia, J. Gonzalez-Rodriguez, H. Fronthaler, K. Kollreider, and J. Bigun. (2007). "A comparative study of fingerprint image-quality estimation methods". Information Forensics and Security, IEEE Transactions on, 2(4), 734-743.
- [12] S.J. Xie, J.C. Yang, S. Yoon, D.S. Park. J. W. (2011). "Fingerprint quality analysis and estimation for fingerprint matching". State of the art in Biometrics. Intech, Vienna. ISBN, 978-953.
- [13] Y. Chen, S.C. Dass, A.K. Jain. (2005, January). "Fingerprint quality indices for predicting authentication performance". In Audio-and Video-Based Biometric Person Authentication (pp. 160-170). Springer Berlin Heidelberg.
- [14] P. Grother, E. Tabassi. (2007). "Performance of biometric quality measures". Pattern Analysis and Machine Intelligence, IEEE Transactions on, 29(4), 531-543.
- [15] S.J. Xie, S. Yoon, J. Shin, D.S. Park. "Effective fingerprint quality estimation for diverse capture sensors". Sensors 10.9 (2010): 7896-7912.
- [16] ISO/IEC 29794–4. 2010. Information technology – biometric sample quality – part 4: finger image data.
- [17] ISO/IEC 19794–1. 2011. Information technology – biometric data interchange formats – part 1: framework.
- [18] L.L. Shen, A. Kot, W.M. Koo. "Quality measures of fingerprint images." Audio-and Video-based Biometric Person Authentication. Springer Berlin Heidelberg, 2001.
- [19] K. Phromsuthirak, V. Areekul. "Fingerprint quality assessment using frequency and orientation subbands of block-based fourier transform". Biometrics (ICB), 2013 International Conference on. IEEE, 2013.
- [20] M.A. Olsen, H. Xu, C Busch. "Gabor filters as candidate quality measure for NFIQ 2.0". Biometrics (ICB), 2012 5th IAPR International Conference on. IEEE, 2012.
- [21] E. Tabassi, C.L. Wilson. "A novel approach to fingerprint image quality." Image Processing, 2005. ICIP 2005. IEEE International Conference on. Vol. 2. IEEE, 2005.
- [22] NIST. Development of NFIQ 2.0, Accessed: 2014-05-03. http://www.nist.gov/itl/iaid/ig/development_nfig_2.cfm.
- [23] C Lee, S Lee, J Kim. "A study of touchless fingerprint recognition system." Structural, Syntactic, and Statistical Pattern Recognition. Springer Berlin Heidelberg, 2006. 358-365.
- [24] MO Derawi, B Yang, C Busch. "Fingerprint recognition with embedded cameras on mobile phones." Security and Privacy in Mobile Information and Communication Systems. Springer Berlin Heidelberg, 2012.
- [25] P. Vincenzo, and F. Scotti. "Fingerprint biometrics via low-cost sensors and webcams." Biometrics: Theory, Applications and Systems, 2008. BTAS 2008. 2nd IEEE International Conference on. IEEE, 2008.
- [26] B. Yang, X. Li, and C. Busch. 2012. "Collecting fingerprints for recognition using mobile phone cameras." In IS&T/SPIE Electronic Imaging.
- [27] G. Li, B. Yang, R. Raghavendra, and C. Busch. 2012. "Testing mobile phone camera based fingerprint recognition under real-life scenarios." Norsk informasjonssikkerhetskonferanse (NISK).
- [28] G. Li, B. Yang, M. A. Olsen, and C. Busch. 2013. "Quality assessment for fingerprints collected by smartphone cameras." In Conference on Computer Vision and Pattern Recognition Workshops (CVPRW).
- [29] B. Yang, G. Li, and C. Busch. "Qualifying fingerprint samples captured by smartphone cameras." ICIP. 2013.
- [30] TST BiRD 3, Accessed: 2014-05-03. <http://www.neurotechnology.com/fingerprint-scanner-tst-biometrics-bird-3.html>.
- [31] Neurotechnology fingerprint SDK, Accessed: 2014-05-03. <http://www.neurotechnology.com/verifinger.html>.
- [32] D Shaked, I Tastl. "Sharpness measure: Towards automatic image enhancement." Image Processing, 2005. ICIP 2005. IEEE International Conference on. Vol. 1. IEEE, 2005.
- [33] A.M. Bazen, and H.G. Sabih. "Directional field computation for fingerprints based on the principal component analysis of local gradients." Proceedings of ProRISC2000, 11th Annual Workshop on Circuits, Systems and Signal Processing. Veldhoven, the Netherlands, 2000.
- [34] Autocorrelation, Accessed: 2014-05-03. <http://en.wikipedia.org/wiki/Autocorrelation>.
- [35] Fingerprint enhancement implementation, Accessed: 2014-05-03. <http://www.csse.uwa.edu.au/~pk/research/matlabfns/>.
- [36] F. Tomaz, C. Tiago, and S. Hamid. "Fast and accurate skin segmentation in color images." Computer and Robot Vision, 2004. Proceedings. First Canadian Conference on. IEEE, 2004.